The International Journal of Advanced Manufacturing Technology (2018) 98:1237–1251
https://doi.org/10.1007/s00170-018-2294-1

ORIGINAL ARTICLE

# Investigation of cutting forces, surface integrity, and tool wear when high-speed milling of high-volume fraction $SiC_p$/Al6063 composites in PCD tooling

Junfeng Xiang [1] · Siqin Pang [1,2] · Lijing Xie [1,2] · Xin Hu [1] · Song Peng [1] · Tao Wang [1]

Received: 23 January 2018 / Accepted: 5 June 2018 / Published online: 18 June 2018


**Abstract**
This paper focused on high-speed milling of Al6063 matrix composites reinforced with high-volume fraction of small-sized SiC particulates and provided systematic experimental study about cutting forces, thin-walled part deformation, surface integrity, and tool wear during high-speed end milling of 65% volume fraction $SiC_p$/Al6063 (Al6063/$SiC_p$/65p) composites in polycrystalline diamond (PCD) tooling. The machined surface morphologies reveal that the cutting mechanism of SiC particulates plays an important role in defect formation mechanisms on the machined surface. In high-speed end milling of Al6063/$SiC_p$/65p composites, the cutting forces are influenced most considerably by axial depth of cut, and thus the axial depth of cut plays a dominant role in the thin-walled parts deformation. Increased milling speed within a certain range contributes to reducing surface roughness. The surface and sub-surface machined using high-speed milling suffered from less damage compared to low-speed milling. The milling speed influence on surface residual stress is associated with milling-induced heat and deformation. Micro-chipping, abrasive wear, graphitization, grain breaking off, and built-up edge are the dominated wear mechanism of PCD tools. Finally, a series of comparative experiments were performed to study the influence of tool nose radius, average diamond grain size, and machining parameters on PCD tool life.

**Keywords** High-speed milling · $SiC_p$/Al6063 composites · Cutting forces · Surface integrity · Tool wear · PCD tooling

## 1 Introduction

In recent years, SiC particulates reinforced aluminum composites ($SiC_p$/Al) are considered to have great potential industrial applications due to their superior properties, such as high strength to weight ratio, high stiffness, low-temperature sensitivity, and high resistance to wear, which make them superior to unreinforced alloys. Based on its special commercial and technological importance, $SiC_p$/Al composites are rapidly replacing conventional materials in the aerospace, automotive, electronics, infrastructure, and medical industries [1–3]. However, due to their low plasticity, non-uniformity, and abrasive nature of SiC reinforcement, it is still a challenge to achieve a good surface quality of $SiC_p$/Al composites by conventional machining methods. Especially due to the presence of rigid ceramic particulates in the soft Al alloy matrix which leads to rapid tool wear, which limits its widespread engineering application [4]. Although many engineering components made from $SiC_p$/Al composites can be produced using the near net shape forming and casting processes, final machining process is still inevitable in order to achieve the final dimensions [5]. Therefore, a deep understanding of the influence of machining technologies and process parameters on the machining quality and tool wear is of great practical value for widespread applications of $SiC_p$/Al composites.

Over the past two decades, the machining of difficult-to-cut $SiC_p$/Al composites has drawn great attention in both academic and industrial fields. Chan et al. [6] investigated surface formation in ultra-precision diamond turning of Al6061/15SiC and found that the machining quality could be significantly improved by using high spindle speed and fine tool

✉ Lijing Xie
rita_xie2004@163.com

[1] School of Mechanical Engineering, Beijing Institute of Technology, Beijing 100081, China

[2] Key Laboratory of Advanced Machining, Beijing Institute of Technology, Beijing 100081, China

feed rate, but depth of cut appeared not to be the main factor affecting the surface roughness except under low spindle speed condition. Pramanik et al. [7] conducted a study of cutting 20 vol% $SiC_p$/Al6061 specimen with varied machining parameters and found that the surface roughness was mainly controlled by feed rate, while the influence of cutting speed was almost negligible. Ge et al. [8] conducted ultra-precision turning experiments on $SiC_p$/2024Al and $SiC_p$/ZL101A composites and found that surface quality decreased with increasing feed rate and SiC volume fraction, and lower surface roughness values could be produced when a positive cutting edge inclination, zero rake angle, or big flank angle was chosen. Reddy et al. [9] carried out end milling experiments on 20 wt% $SiC_p$/Al composite and investigated the influence of feed rate and milling speed on surface integrity. Quan [10] analyzed the machining effect on the surface hardness of Al/$SiC_p$/15p and concluded that the hardness of the machined surface may be lower than that of the unaffected interior material. By performing high-speed turning of Al/20SiC composites under different cutting parameters, El-Gallab and Sklad [11, 12] studied the effects of feed rate and cutting speed on subsurface damage and surface quality, and found that polycrystalline diamond (PCD) tool can achieve a longer tool life than other tools. Li et al. [13] conducted turning experiments of Al/$SiC_p$/5p composites using coated carbide tool and revealed the influence of cutting speed on tool wear and the main wear mechanisms on flank face. When turning Al/$SiC_p$/10p and Al/$SiC_p$/30p composites using different geometrical CBN tools, Dabade et al. [14] reported that the wiper geometry on the inserts can reduce surface damage and lower cutting forces. The influence of size, volume fraction, and spatial distribution of reinforcement phase on the $SiC_p$/Al composites' machinability characteristics such as cutting forces, surface roughness, residual stress, chip morphology, and shear and friction angles had been also studied in [15–17].

According to the published reports, most of the research works still focus on turning and low volume fraction (< 30%) $SiC_p$/Al composites. In terms of the machining operations, end milling is one of the most widely used metal removal operation in practical production since it is of great capability to yield a high material removal rate and achieve good surface quality. It finds the widespread applications in industries such as the aerospace and automotive industries, where surface quality is an important factor in the production of slots, pockets, precision molds, and dies [18]. In terms of high volume fraction, there exist some applications of $SiC_p$/Al composites with high reinforcement volume fraction in electric packaging and satellites due to its low thermal expansion and high thermal conductivity [19]. Although Huang et al. [20] and Bian et al. [21] conducted high-speed milling experiments of high-volume fraction (up to 56 and 65%) $SiC_p$/Al composites, the SiC particulate size was relatively large (about 60–80 μm).

To the best of the authors' current knowledge, less report about milling high volume fraction $SiC_p$/Al composite with small reinforcement size (less than 10 μm) had been reported unit now. In addition, there are contradictory conclusions about influence of machining parameters on the machining quality in the published reports. Due to the fact that high-speed machining of metal matrix composites reinforced by high volume fraction (over 55 vol%) of particulates was seldom reported, this paper focused on Al matrix composites reinforced with high volume fraction of small-sized SiC particulates and provided systematic experimental study about cutting forces, thin-walled part deformation, surface integrity, tool wear during high-speed milling of 65% volume fraction $SiC_p$/Al6063 composites (Al6063/$SiC_p$/65p) in PCD tooling. To achieve the improvement of the machinability of $SiC_p$/Al6063 composites in practical production, a series of comparative tool life experiments were performed to select the optimized tool nose radius and the tool material grain size. The corresponding tool wear morphology was observed as well. The influence of high-speed milling parameters on the cutting forces was investigated and combined with finite element method to analyze the thin-walled part deformation. The influence of high-speed milling parameters on the surface integrity of Al/$SiC_p$/65p composites was investigated by analyzing the surface roughness, the residual stress and the morphology of machined surface.

## 2 Experimental procedure

### 2.1 Materials

Al6063/$SiC_p$/65p composites were fabricated using vacuum infiltration approach. The chemical composition and material properties of Al6063/$SiC_p$/65p composites were given in Tables 1 and 2, respectively. The compressive yield strength of Al6063/$SiC_p$/65p composites and unreinforced Al6063 alloy were 529 and 228 MPa, respectively [22]. From the microstructure of Al6063/$SiC_p$/65p composites in Fig. 1, it can be observed that the SiC particulates with many sharp corners are approximately polyhedral and the average SiC particulate size are about 5 μm. Due to highly abrasive characteristics of $SiC_p$/Al composite that caused very severe wear on carbide tools, PCD tools were recommended by Xiang [23] and Wang [24] who studied the machinability and tool performance of $SiC_p$/Al composites to machine these materials so as to achieve long tool life and acceptable machining quality. Therefore, PCD tools were utilized in this work.

### 2.2 Experimental setup and measurement

The high-speed milling experiments of Al6063/$SiC_p$/65p composites in PCD tooling were conducted on DMU80 mono

**Table 1** Chemical composition of Al6063/$SiC_p$/65p composites

| Element | Al | Mg | Cu | Si | C | Others |
|---|---|---|---|---|---|---|
| Wt% | 38.33 | 0.48 | 1.51 | 51.24 | 8.43 | margin |

BLOCK machining center. The end milling tools, which consist of two PCD inserts brazed on the carbide tool shank, are utilized. The schematic of the milling process for Al6063/$SiC_p$/65p composites is shown in Fig. 2. The research of Kannan [25] reported that the application of coolant would cause the loosely bonded particulates to be flushed away and further result in a higher percentage of voids and pits formed on machined surface. Therefore, all the milling experiments in this paper were performed in dry conditions. The details of tooling and cutting conditions are listed in Table 3.

The milling operation was interrupted periodically in order to examine the machined surface integrity and tool wear. The milling force components ($F_x$, $F_y$, $F_z$) were collected utilizing a triaxial piezoelectric dynamometer (Kistler-9257B). The deformation of thin-walled part was measured by Zeiss Stereo Discovery V12 Stereomicroscope. Regarding surface roughness, since $R_a$ was still widely utilized to evaluate the machined surface quality of $SiC_p$/Al composites [7, 9, 10, 14], $R_a$ was adopted as a measurement standard of surface roughness in this paper. Measuring surface roughness was achieved by Talysurf CCI non-contact surface profiler system. Based on the machined surface roughness range, the cutoff length was set to 0.8 mm and the evaluation length was equal to 4.0 mm according to ISO 4288. The final value of surface roughness under each parameter combination were determined by measuring five locations in feed direction and then averaging them. The schematic of surface roughness measuring approach was demonstrated in Fig. 3.

After completing machining experiments, the worn tool morphology and machined surface were examined by scanning electron microscopy (SEM) and VK-X200 3D laser scanning microscope (LSM). Since there is no published standard for measuring the residual stress on this material, the residual stress measurements were all made on the machined surface along the feed direction using x-ray diffraction sin2$\psi$ technique. In addition, Al{2 2 2} crystal surface and CrK$\alpha$ target were selected. The results averaged the residual stress values of three different locations under each set of milling condition.

**Table 2** Material properties of Al6063/$SiC_p$/65p composites

| Material properties | Value |
|---|---|
| Density (kg/m$^3$) | 2960 |
| Specific heat capacity (J/kg °C$^{-1}$) | 750 |
| Coefficient of thermal expansion (°C$^{-1}$) | $7.7 \times 10^{-6}$ |
| Thermal conductivity (W/m °C$^{-1}$) | 175 |
| Volume fraction of SiC (vol%) | 65 |
| Average particulate size (μm) | 5 |
| Elastic modulus (GPa) | 221 |
| Poisson's ratio | 0.21 |
| Melting point | 635 |

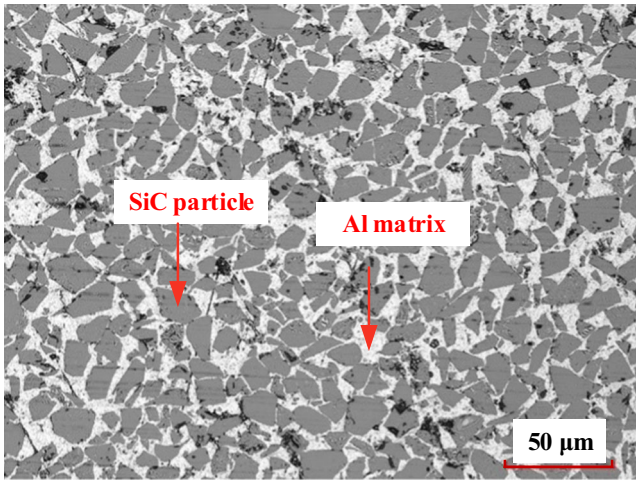


**Fig. 1** Micrograph of Al6063/$SiC_p$/65p composites

## 3 Machined surface formation mechanisms

Since knowledge of surface formation mechanisms is important and necessary for improving Al6063/$SiC_p$/65p composites' machinability, the machined surface formation mechanisms are firstly investigated. During high-speed milling of $SiC_p$/Al composites, soft Al matrix and hard SiC particulates are cut alternately, thereby causing the vibration of milling tool during cutting process. The formation of milled surface is not only influenced by the combination movement of feed rate and milling speed but also influenced greatly by hard SiC particulates in the workpiece.

Figure 4 shows the machined surface morphology of Al6063/$SiC_p$/65p composites. The machined surface morphologies of Al6063/$SiC_p$/65p composites are characterized by shallow pits caused by fractured or crushed SiC particulates, swelling formed by pressed-in SiC particulates, big cavities formed from pulled-out SiC particulates, and high-frequency scratch of SiC particulates. Figure 4a shows the macroscale milled surface morphology. Except the pitches generated by feed movement, many pits with the size around 10–20 μm are randomly distributed on it. In Fig. 4b, the bottom surfaces of the two pits on the left side are quite rough, which indicates the occurrence of SiC fracture. There are obvious cracks formed perpendicular to cutting direction, which can be attributed to the smearing phenomenon. Due to high temperature generated during the high-speed milling process, Al matrix often experienced side flow and smearing on the defect regions. Due to high plasticity of Al matrix and

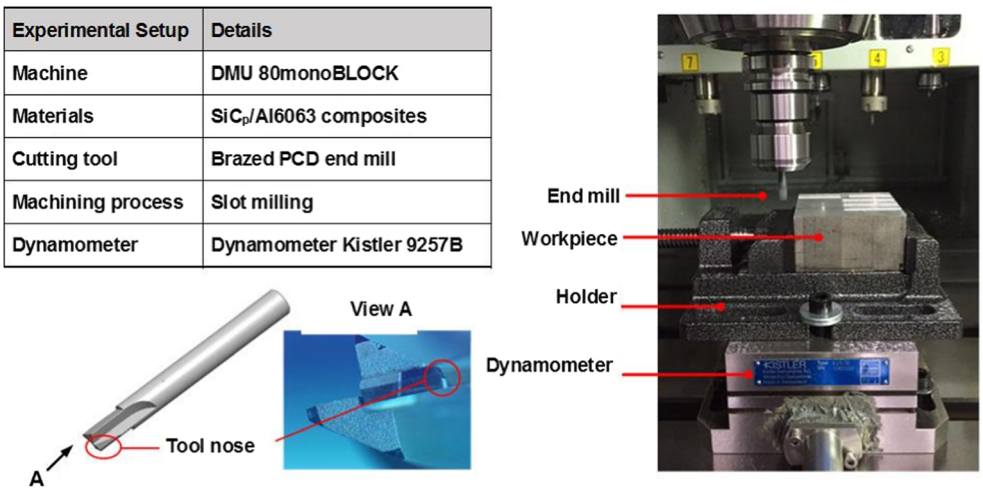


**Fig. 2** Schematic of milling process for Al6063/$SiC_p$/65p composites

softening effect under milling-induced high temperature, smearing is a very common phenomenon during high-speed milled Al6063/$SiC_p$/65p composites. The smearing phenomenon might improve the surface quality to some extent. Further magnification of one pit is shown in Fig. 4c where many SiC particulates with the size around 0.4–0.9 μm were distributed on the bottom surface. Since the average size of SiC reinforcement is about 5 μm, it is assumed that these small SiC particulates were formed by SiC particulate fracture during milling process. The voids were formed due to strain hardening of the material, i.e., dislocation pile-up in Al matrix that surrounds rigid SiC particulates. As a result of the interface debonding between SiC particulates and Al matrix, some SiC particulates are easily pulled out of the machined surface, which is also indicated by the presence of small grooves on the machined surface. The formation of these small grooves is due to the fact that SiC particulates were pulled out of aluminum matrix and then dragged over the machined surface, consequently leading to the presence of some scratches, of which the width was about 5 μm close to the average size of SiC particulates. It is worth pointing out that no all the bottom surfaces of pits are quite rough, and Fig. 4d shows a shallow pit with relative smooth bottom surface, which was formed by the rotation of SiC particulate that was originally located on the cutting path. Figure 4e shows that a typical cavity on the machined surface was formed by the pulling out of SiC particulate. After pulling out, some particulates may fall into the regions between tool flank surface of the mill tool and machined surface, which would be pressed into the machined surface and form the swelling, as shown in Fig. 4f.

**Table 3** Summary of experimental details

| Items | Contents |
|---|---|
| Tooling | |
| Tool tip material | Polycrystalline diamond |
| PCD average grain size $D_g$ (μm) | 7.5, 10 |
| PCD nose radius $R_n$ (mm) | 0.1, 0.4 |
| Tool diameter $d$ (mm) | 6 |
| Rake angle (°) | 2 |
| Clearance angle (°) | 10 |
| Tool cutting edge angle (°) | 90 |
| Workpiece | |
| Material | Al6063/$SiC_p$/65p composites |
| Thickness (mm) | 2 |
| Cutting conditions | |
| Operation | End milling |
| Cutting speed $V_c$ (m/min) | 100, 170, 240, 300, 380, 400, 500 |
| Feed rate $f_z$ (mm/rev) | 0.02, 0.025,0.04, 0.05, 0.06, 0.075, 0.08, 0.1 |
| Axial depth of cut $a_e$ (mm) | 0.02, 0.05, 0.075, 0.1, 0.125, 0.15 |
| Cutting environment | Dry |

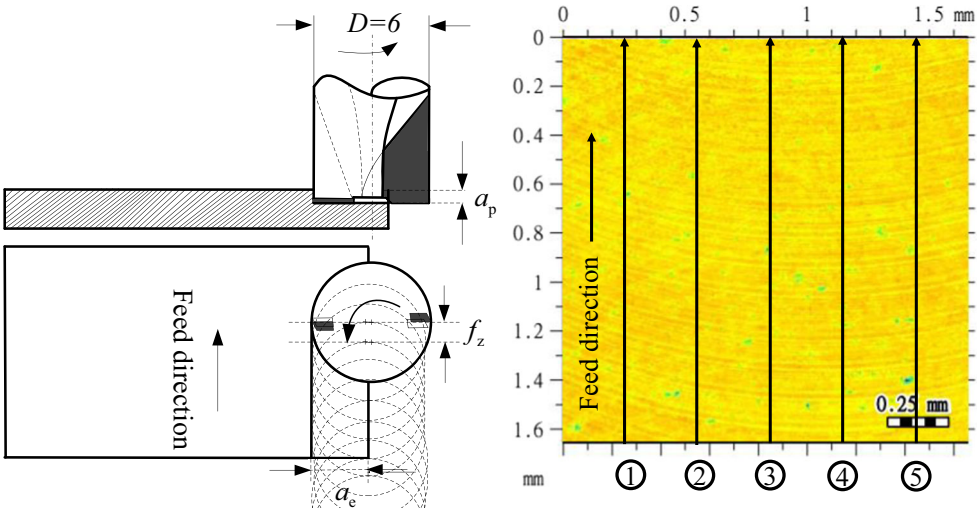


**Fig. 3** Schematic of surface roughness measuring approach

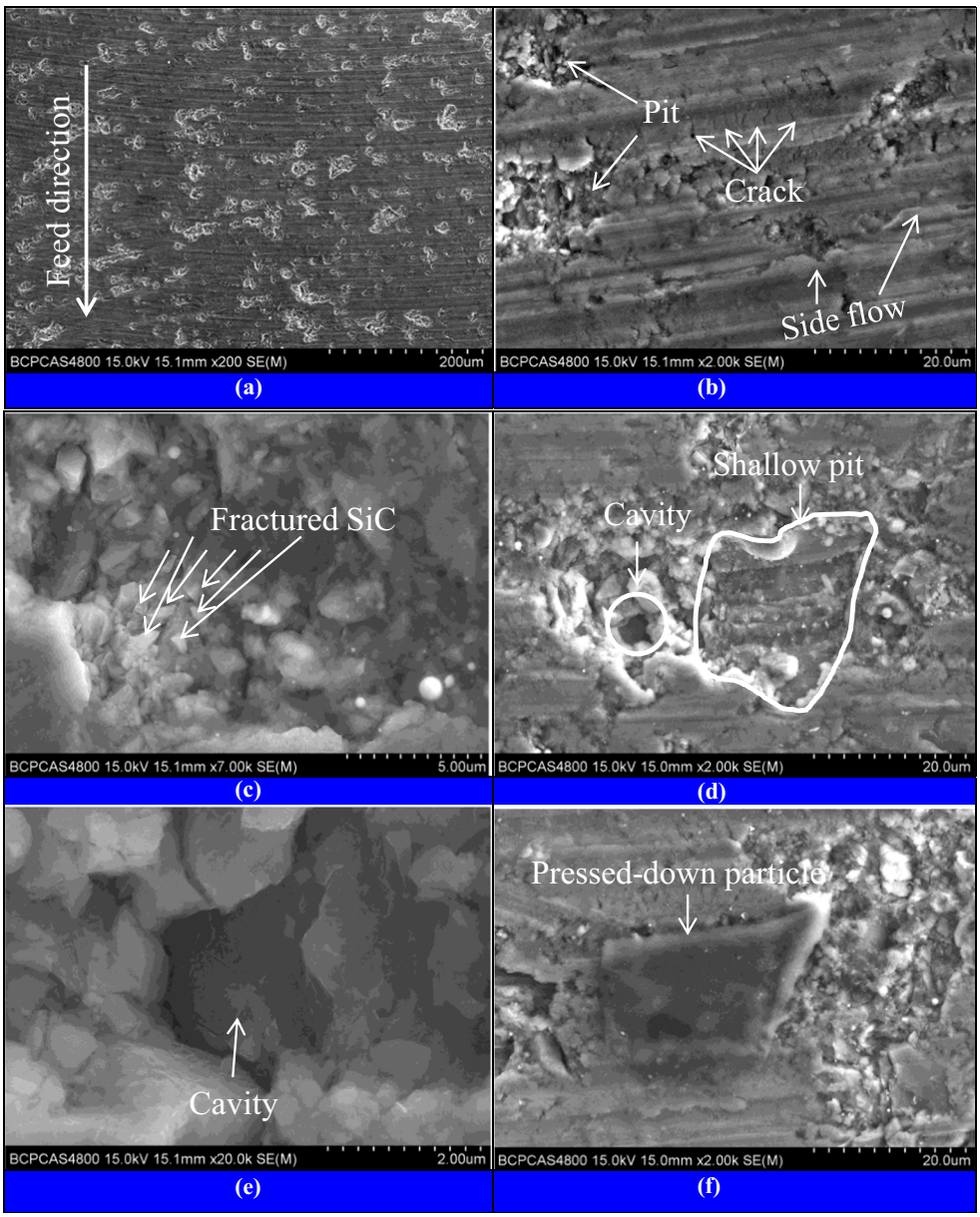


**Fig. 4** SEM micrograph of the machined surface ($v_c = 300$ m/min, $a_p = 0.05$ mm, $a_w = 6$ mm, $f = 0.04$ mm/rev). **a** Macro-machined morphology. **b** Scratch and micro-crack. **c** Cavity formed by SiC cracking. **d** Shallow pit caused by SiC scratch. **e** Cavity formed by pulled-out SiC particulate. **f** Swelling caused by pressed-in SiC particulate

According to the machined surface formation analysis above, the cutting mechanism of SiC particulate plays an important role in defect formation mechanism on the machined surface. Figure 5a, b shows the surface defects formation before and after cutting, respectively. The rotation, pressed-in, pulled-out and fracture of SiC particulates contribute to the formation of micro-crack, pits, swelling, and cavities.

## 4 Results and discussion

### 4.1 Milling forces

The measurement of milling force components is highly essential for analyzing the machinability of Al6063/$SiC_p$/65p composites. Figure 6 shows the influence of the feed rate, axial depth of cut, and milling speed on milling forces during high-speed milling of Al6063/$SiC_p$/65p composites. All the milling forces are increased by feed rate and axial depth of cut. The force $F_z$ along the $z$ direction normal to the milling surface decreases with the milling speed increasing from 100 to 300 m/min and then increases with the milling speed. This is due to the fact that high-speed-milling-induced higher temperature further intensified the softening effect of Al matrix. It is worth noting that the influence of milling speed on the milling forces is the smallest compared to that of the other two machining parameters.

The machining deformation of thin-walled Al6063/$SiC_p$/65p parts was investigated by finite element method using the material properties of Al6063/$SiC_p$/65p composites in Table 2 and the milling forces obtained experimentally. The research of Mondal [26] found that the deformation of $SiC_p$/Al composites is not sensitive enough to temperature. The key to reducing the deformation of thin-walled parts is to increase the rigidity of the thin-walled part and to reduce the cutting forces. When finish machining thin-walled parts, increasing the axial depth of cut can increase the rigidity of thin-walled pieces, with a concomitant increase of the milling forces, so the choice of axial depth of cut is very important for controlling the machining induced deformation of thin-walled parts. Since the machining-induced deformation in the end milling is mainly manifested as the deformation perpendicular to the machined surface of the thin-walled parts, only the milling

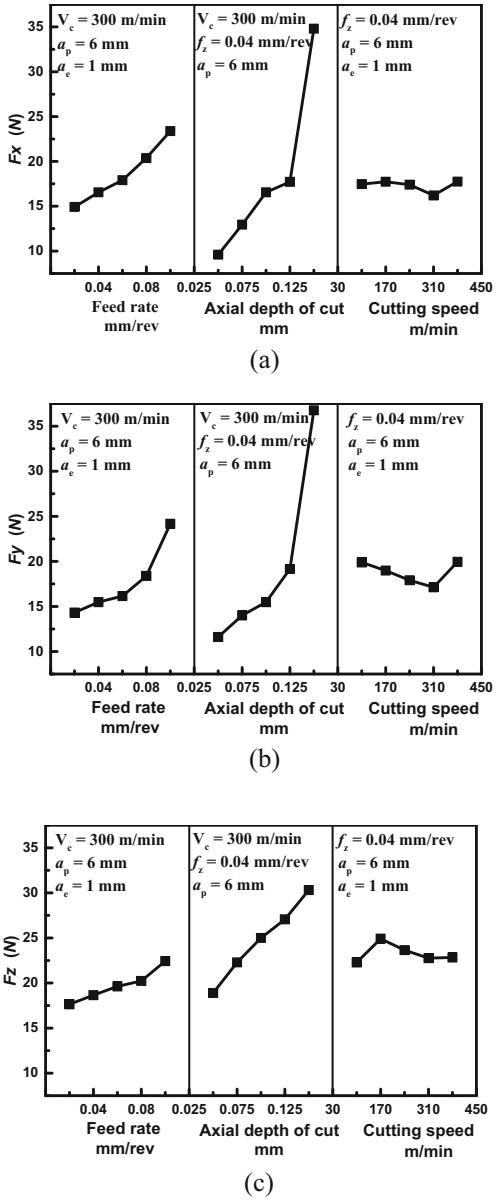


**Fig. 6** Influence of the feed rate, axial depth of cut, and milling speed on milling forces. **a** Force $F_x$ along the $x$ direction. **b** Force $F_y$ along the $y$ direction. **c** Force $F_y$ along the $z$ direction

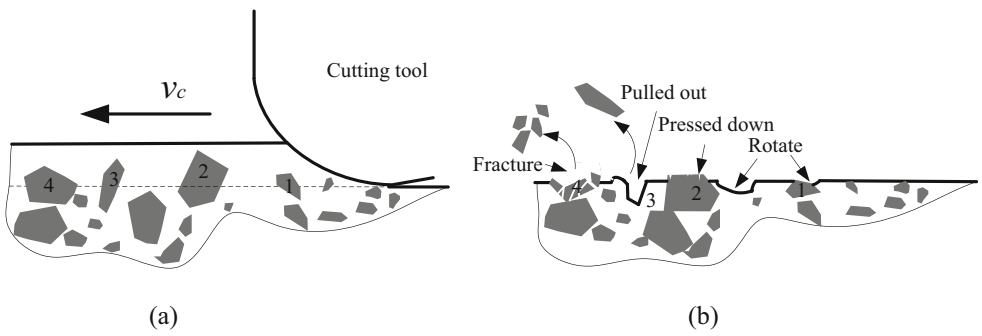


**Fig. 5** Schematic of machined surface formation mechanism. **a** Before cut. **b** After cut

force along the $z$ direction perpendicular to the machined surface is adopted in the FE simulation.

The forces $F_z$ along the direction normal to the milling surface were measured to be 66.31 and 39 N by repeating the same milling tests multiple times under the axial depth of cut of 0.05 and 0.02 mm, respectively. The machining induced deformation of thin-walled parts is calculated by running FE model with the applied stress that is equal to the force $F_z$ divided by cross-sectional area of the tool bottom. When the axial depth of cut is, respectively, 0.05 and 0.02 mm, the experimental and simulated deformation results of thin-walled parts are shown in Fig. 7 where the experimentally observed deformation is the total deformation of two same samples machined under the same machining parameters. The comparison of thin-walled parts deformation between experiment and FE simulation under different axial depths of cut is presented in Table 4. The relative errors of thin-walled parts deformation determined experimentally and numerically under different axial depths of cut are both less than 17% and the simulated deformation shows a fairly good agreement with the experimental observation. This indicates that the axial depth of cut plays a dominant role in the thin-walled parts deformation when high-speed end milling Al6063/$SiC_p$/65p composites.

**Table 4** Comparison of thin-walled parts deformation between experiment and FE simulation

| Axial depth of cut | Experiment deformation | Simulated deformation | Relative error |
|---|---|---|---|
| 0.02 | 0.012 | 0.014 | 14.3% |
| 0.05 | 0.028 | 0.024 | 16.7% |

## 4.2 Surface integrity

After conducting high-speed milling experiments, the corresponding machined surface roughness under various milling parameters combination was measured. The roughness values *Ra* of machined surface obtained using PCD tools with tool nose radius of 0.1 and 0.4 mm are given in Fig. 8. At the beginning stage of end milling, the surface roughness values have a fluctuation for a short distance due to rapid wear of sharp cutting edge in the PCD tooling. However, with increasing cutting time and resultant tool wear, the extrusion and friction between the flank face and the machined surface are greatly increased. Therefore, the actions of extrusion and friction on the machined surface lead to an increase in surface roughness. The surface roughness of the Al6063/$SiC_p$/65p workpiece machined using 0.1-mm tool nose radius is slightly

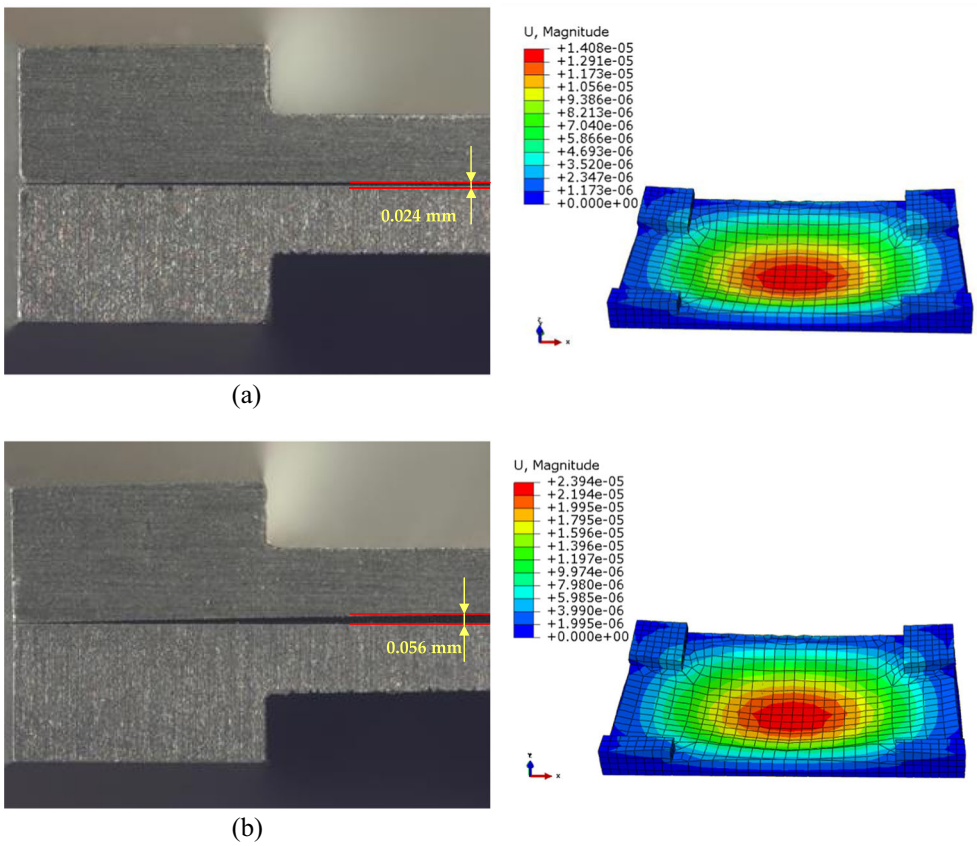


**Fig. 7** Experimental (left) and simulated (right) deformation results of thin-walled parts under different axial depths of cut. **a** Axial depth of cut 0.02 mm. **b** Axial depth of cut 0.0.5 mm

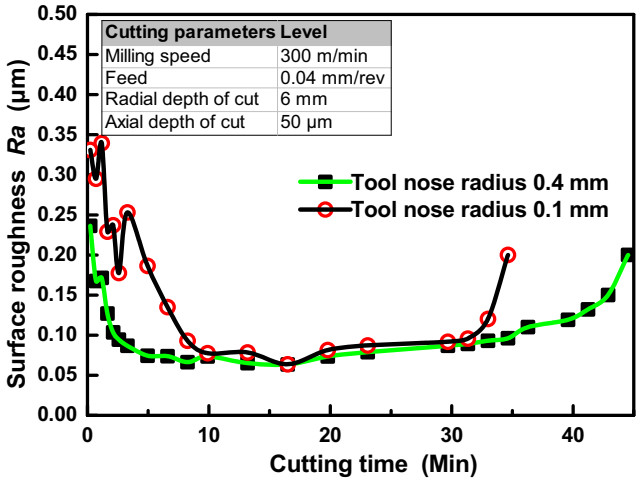


**Fig. 8** Influence of tool nose radius on the surface roughness

higher than that using 0.4 mm tool nose radius, as shown in Fig. 8.

The influence of feed rate, cutting speed, and axial depth of cut on surface roughness *Ra* is presented in Fig. 9. The influence of feed rate and axial depth of cut, especially feed rate on surface roughness, are very significant. The increase in feed rate can lead to the increase in the pitch of machined surface morphology, thereby increasing the surface roughness. When large axial depth of cut is utilized, high cutting forces are generated, which would deteriorate the surface roughness and lead to increased surface roughness. Experimental results indicate that the surface roughness *Ra* increase with feed rate and axial depth of cut. When the feed rate increase from 0.02 to 0.1 mm/rev, the surface roughness values increase by 100%, which can be explained by the corresponding SEM micrographs of the machined surface morphology varying with feed rate in Fig. 10.

As for milling speed, its influence on surface roughness is relatively complex. When high-speed milling is utilized, the machining process tends to be more adiabatic and the heat

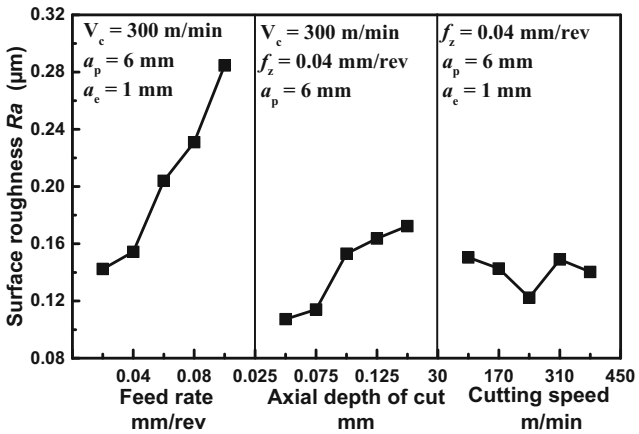


**Fig. 9** Influence of feed rate, cutting speed, and axial depth of cut on surface roughness *Ra*

generated in the cutting zone does not have enough time to conduct away, thereby increasing cutting temperature. High temperature can soften matrix material and increase its flowability. Therefore, SiC particulates are more likely to rotate and pull out, as showed in Fig. 4d, e, and when these pulled out SiC particulates interact with the cutting tool, more pits are formed on the machined surface, thus increasing surface roughness. The following two factors may concurrently influence the surface roughness during high-speed milling. One is that high temperature generated in high-speed milling can aid in grain boundary dislocations, which would reduce the surface roughness within a certain range and increase the surface roughness beyond this range [9]. The other one is that low flowability during high-speed milling make SiC particulates more likely to be cut through, which can reduce surface roughness [6]. Therefore, the final influence of milling speed on surface roughness is the combined actions of the above two factors, and increased milling speed within a certain range contributes to reducing the surface roughness, but would increase the surface roughness beyond this range.

In order to further investigate the interactive influence of any two process variables on surface roughness, both contour plots and surface plots are drawn for three different combinations of milling parameters, as shown in Fig. 11. Figure 11a demonstrates the interactive influence of milling speed and feed rate on surface roughness. Since the interactive action between milling speed and feed rate on surface roughness is significant, the response surface is twisted correspondingly. Under the fixed feed rate, the machined surface roughness decreases with increasing milling speed when the feed rate is at low values (lower than around 0.035 mm/rev), while the trend reverses when feed rate increases to around 0.035–0.05 mm/rev. Under the fixed milling speed, the machined surface roughness increases with feed rate when the milling speed was relatively high, while the decrease trend becomes considerable when the milling speed decreases to about 100 m/min. The interactive effects of milling speed and axial depth of cut, axial depth of cut, and feed rate on surface roughness are, respectively, shown in Fig. 11b, c, where the relatively flat response surfaces indicate the two interaction effects are not significant.

As matrix cracking, cavities caused by fractured or pulled out SiC particulates and interface debonding are involved in the machined surface formation, the surface, and sub-surface damages in the machined Al6063/$SiC_p$/65p composites are expected to occur. Figure 12 shows the machined induced surface and sub-surface damages in the Al6063/$SiC_p$/65p workpiece machined using different milling speeds. Less surface and sub-surface damages are induced by end milling with higher cutting speed of 240 m/min, compared to that of 100 m/min. The difference of different milling speed-induced sub-surface damage in depth might be attributed to surface formation mechanisms under different cutting speeds. Figure 13

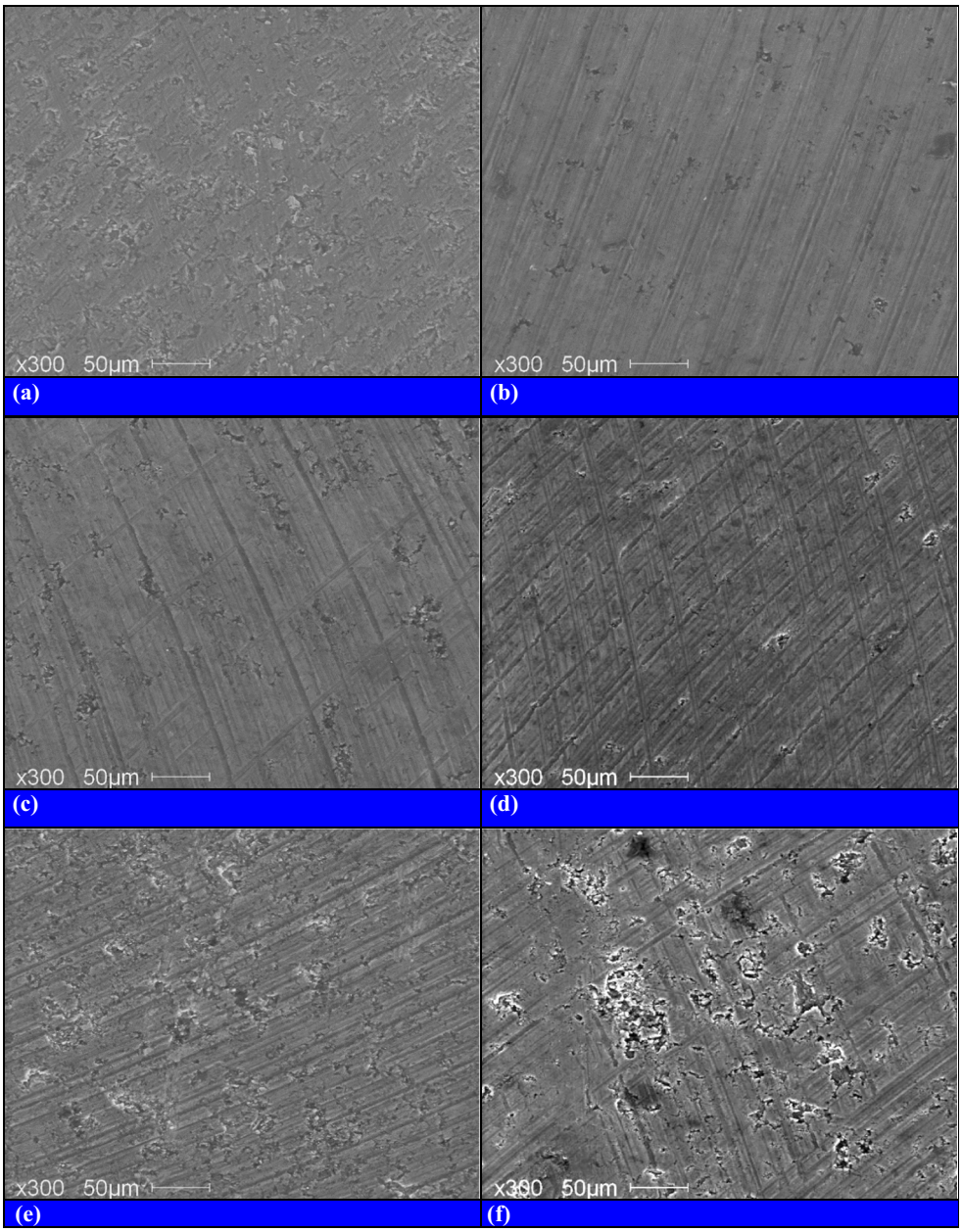


**Fig. 10** Machined surface morphology of Al6063/$SiC_p$/65p workpiece under different feed rates. **a** As received. **b** $f_z$ = 0.02 min/rev. **c** $f_x$ = 0.04 min/rev. **d** $f_x$ = 0.06 min/rev. **e** $f_x$ = 0.08 min/rev. **b** $f_x$ = 0.10 min/rev

clearly shows the surface formation mechanisms at microstructural scale of $SiC_p$/Al composites when subjected to low-speed cutting and high-speed cutting. When performed low-speed cutting of Al6063/$SiC_p$/65p composites, the localized shear applied by removing unmachined surface would lead to the concomitant movement of machined surface and sub-surface due to deformation compatibility and further cause the machined surface and sub-surface damage under combined effects of interface debonding and matrix cracking. While performed high-speed cutting, unlike coordinated deformation of machined surface and sub-surface in low-speed cutting, as the unmachined surface is cut away, the machined surface and sub-surface suffer from less amount of deformation, thereby inducing less damage.

The influence of fate rate, cutting speed, and axial depth of cut on surface residual stress in dry milling of Al6061/$SiC_p$/65p composites are represented in Fig. 14. The milling-induced surface residual stresses of Al6061/$SiC_p$/65p composites are all compressive. The surface residual stress decreases by 81 MPa with feed rate ranging from 0.02 to 0.1 mm/rev, which can be mainly attributed to the fact that the higher feed rate can lead to larger removal rate and resultant higher temperature that is expected to induce tensile stress. The surface residual stress decreases by axial depth of cut, and when the axial depth of cut increases from 0.05 to 0.15 mm, the surface residual stress decreases by 93.5 MPa. When the milling speed increases from 100 to 380 m/min, the surface compressive residual stress first decreases from 113 to 94 MPa and then increases from 94 to

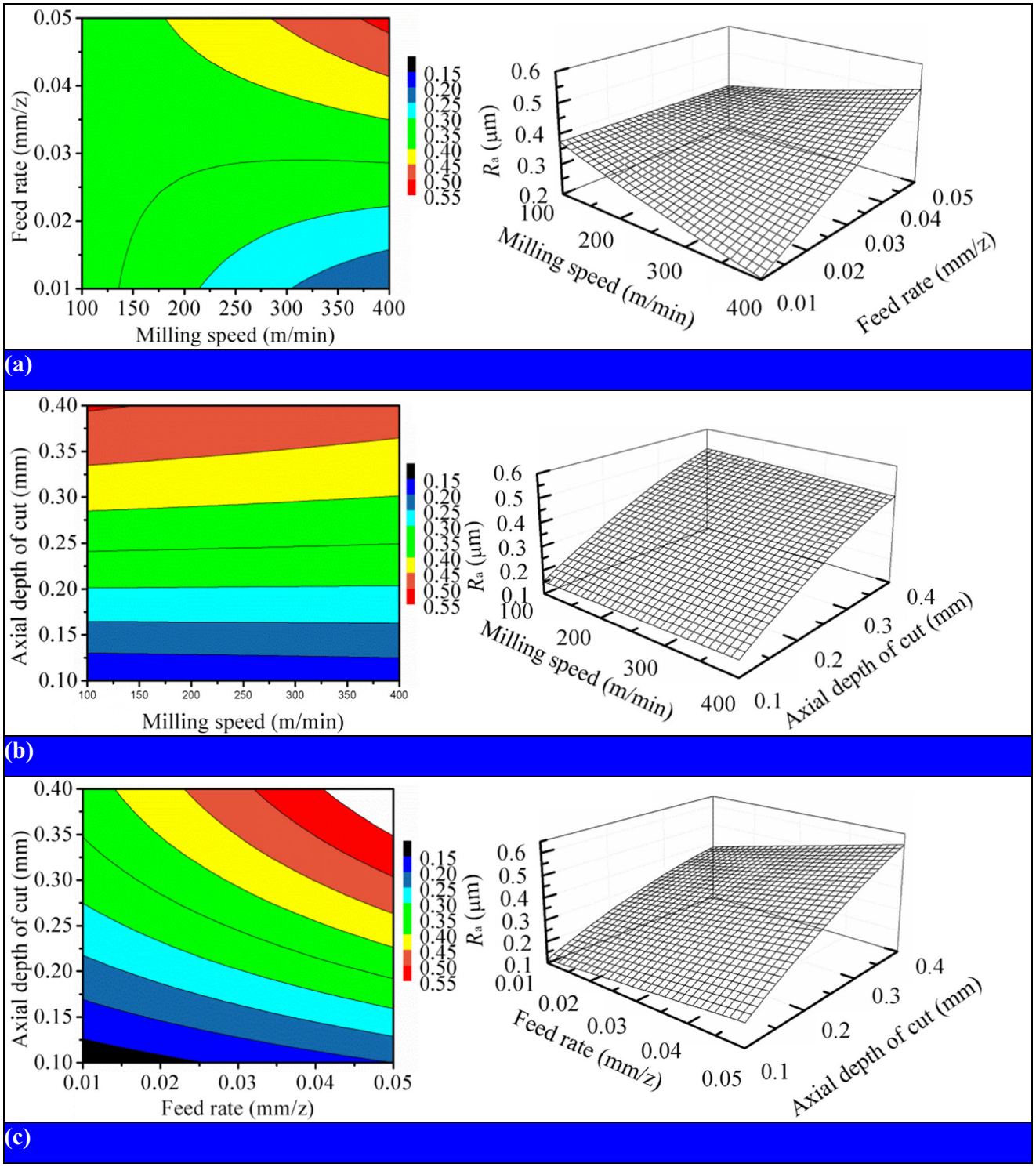


**Fig. 11** Interactive influence of any two process variables on surface roughness. **a** Milling speed vs. feed rate. **b** Milling speed vs. axial depth of cut. **c** Axial depth of cut vs. Feed rate

113.5 MPa. This may be due to the synthetic action of tensile stress caused by heat generated during the milling process and compressive stress originating from mechanical deformation caused by cutting tool. When the milling speed increases from 100 to 240 m/min, high milling speed brings about high-temperature rise that induces tensile stress. When milling speed increases from 240 to 380 m/min, the compressive stress increment induced by tool mechanical action overweighs the tensile stress increment caused by temperature rise during the milling process, and the compressive residual stress increases.

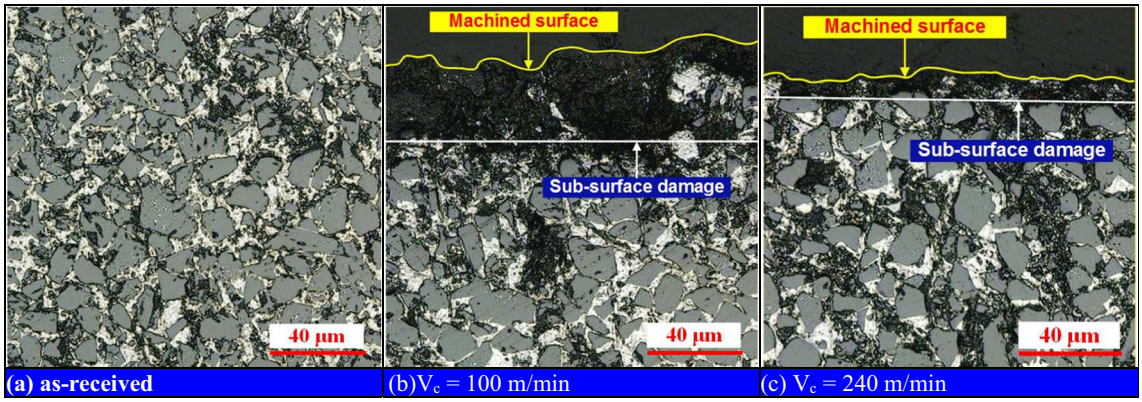


**Fig. 12** Machining induced surface and sub-surface damages in the Al6063/$SiC_p$/65p workpiece machined using different milling speeds

## 4.3 Tool wear

### 4.3.1 Micro-chipping, abrasive wear, graphitization, grain breaking off, and built-up edge

Figure 15 shows the typical wear morphologies of rake face and flank face of PCD tools after dry milling of Al6063/$SiC_p$/65p composites. Under the combined effect of the alternate stress and impact stress, micro-chipping was formed on the cutting edge (Fig. 15a) only if the local stress reached the cleavage strength of PCD tool. Once the micro-chipping occurs, the stress concentration may exist in these regions, which will result in bigger chipping or large-scale fracture. As the pulled-out SiC particulates fall into the tool rake face and flank face, a great amount of two- and three-body abrasion happens. The fine grooves on the flank face of PCD tool indicates the flank face suffered from severe abrasive wear during milling $SiC_p$/Al composites, as shown in Fig. 15b. The occurrence of this phenomenon is due to the abrasive nature of SiC particulates in the Al matrix composites. Although the hardness of PCD tool is several times higher than that of SiC particulates, considerable abrasive wear and Cu-catalyzed chemical wear occurred on PCD tools under extremely high-frequency impact and scrape as well as high-speed milling-induced temperature and pressure. Figure 16 shows the Raman spectra for rake face of PCD tool. The sharp D peak at around 1358 $cm^{-1}$ and G peak at around 1590 $cm^{-1}$ on the rake face of PCD tool imply the transformation of diamond to graphite phases. More details of diamond tools wear during machining of $SiC_p$/Al composites containing Cu are provided in [27].

As the milling process proceeded, the micro-cutting and friction on PCD tool would scrape the Co binder around PCD grains so that Co binder became less and some of diamond grains would be exposed. Due to high-frequency scrape and impact of SiC particulates, these diamond grains due to weakened cohesive strength would be scraped off, and the tool wear morphology after diamond grains were broken off is shown in Fig. 15c. Figure 15d shows the formation of the built-up edge (BUE) on the cutting edge. This is because $SiC_p$/Al composites have all characteristics of strain-hardened two-phase materials under high temperature, high pressure, and high friction that easily lead to BUE. The tool morphologies of PCD tool indicate micro-chipping, abrasive wear, graphitization, grain breaking off, and built-up edge are the dominated wear mechanism of PCD tool in high-speed milling of Al6063/$SiC_p$/65p composites.

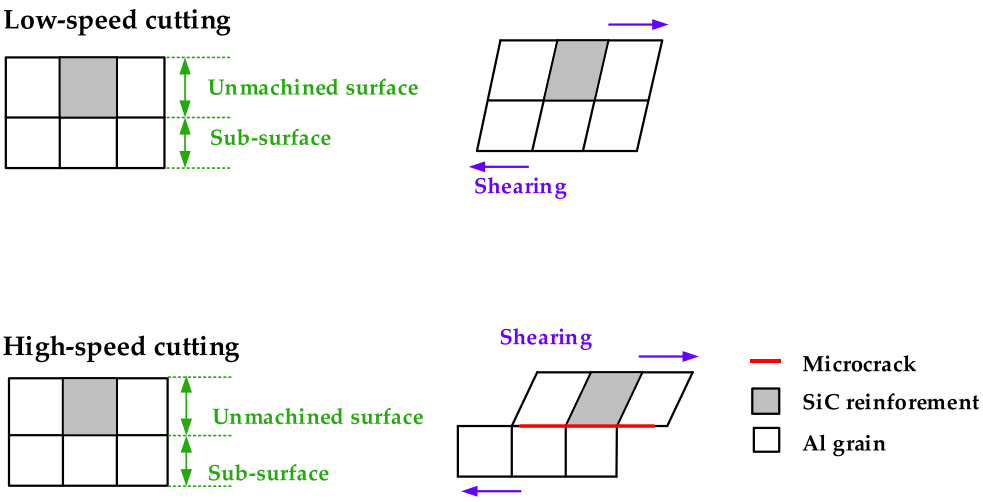


**Fig. 13** Surface formation mechanisms at microstructure scale of $SiC_p$/Al composites when subjected to low-and high-speed cutting

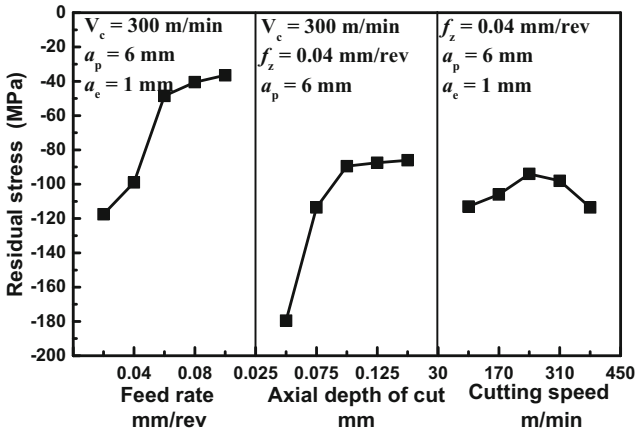


**Fig. 14** Influence of feed rate, cutting speed, and axial depth of cut on surface residual stress

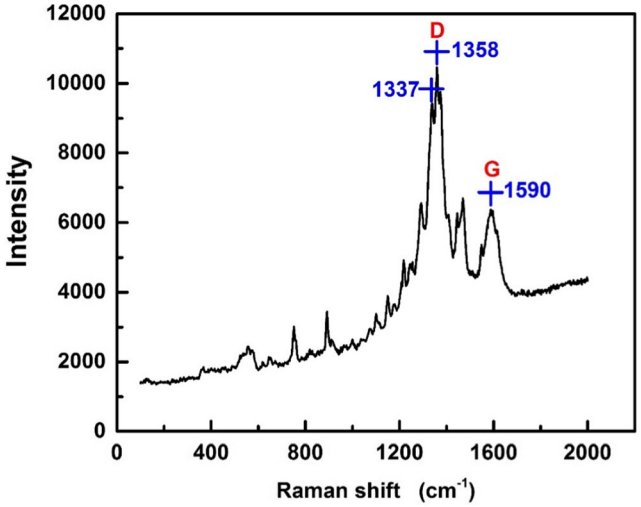


**Fig. 16** Raman spectra for rake face of PCD tool

### 4.3.2 Influence of machining parameters on tool wear

The tool nose radius and grain size play a key role in determining the tool wear modes. Figure 17 shows the influence of tool nose radius and average diamond grain size on the flank wear. Experimental results reveal that PCD tools with a larger nose radius have a longer tool life, and a smaller diamond grain size can effectively extend tool life to some extent. As seen from Fig. 18, the milling speed has a significant influence on PCD tool life. The PCD tools working at the milling speeds of 400 and 500 m/min both suffered from severe wear. The wear curves of PCD tool working under the milling speed 300 m/min experienced obvious initial wear, normal wear, and severe wear stages. The increase of milling speed would increase the number and probability of contact between PCD tool and SiC particulates in the Al6063/$SiC_p$/65p composites. Consequently, the tool flank face suffered from serious abrasion and scrape, correspondingly reducing tool life. The change in milling speed affects the simultaneous changes in milling forces and temperature, so its influence on tool wear and durability is the most pronounced. From the viewpoints of

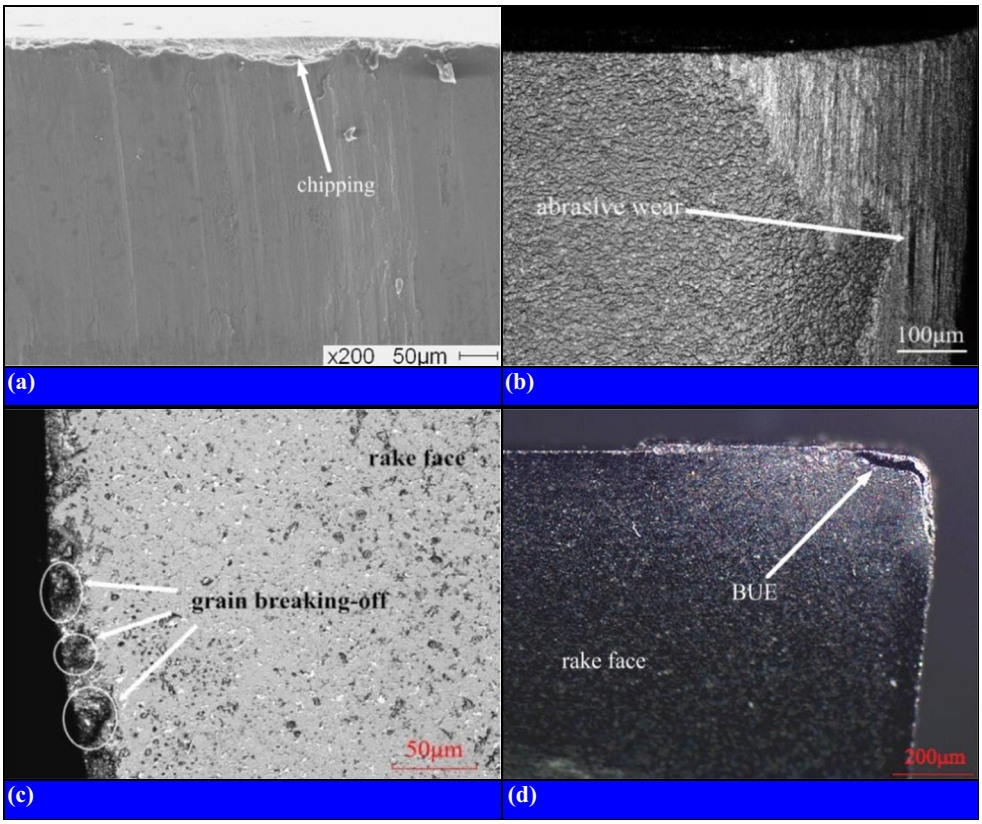


**Fig. 15** Wear morphologies of rake and flank face of PCD tools after dry milling of Al6063/$SiC_p$/65p composites. **a** Micro-chipping on the flank face. **b** Abrasive wear on the flank face. **c** Grain breaking off. **d** Built-up edge

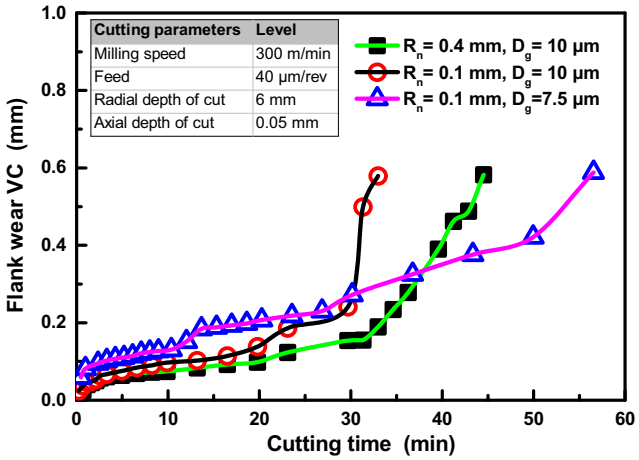


**Fig. 17** Influence of tool nose radius and tool grain size on flank wear

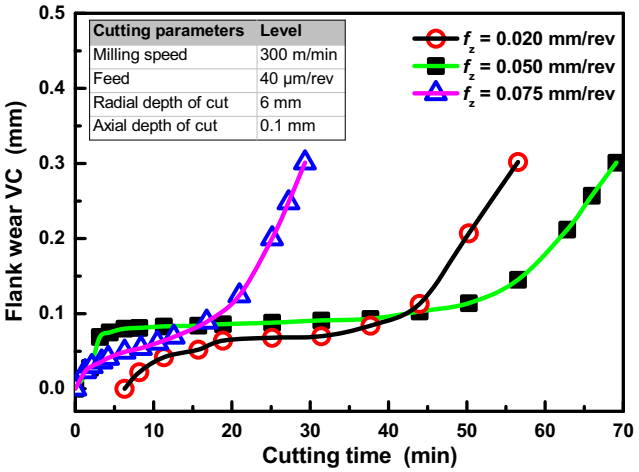


**Fig. 19** Influence of feed rate on flank wear

balancing machining cost and parts quality, it is feasible to select an optimal milling speed such as 300 m/min when high-speed milling of high-volume fraction $SiC_p$/Al6063 composites in PCD tooling.

It is generally assumed that the increase of feed rate would reduce the tool life, and so the tool life under the feed rate of 0.075 mm/rev was is less than half of the tool life under 0.05 mm/rev (Fig. 19). However, the service life of PCD tool working at the feed rate of 0.05 mm/rev is slightly higher than that under the feed rate of 0.02 mm/rev, and the lower feed rate does not improve the PCD tool life. This may be partly due to the reduced probability of contact between SiC particulates and the tool flank under higher feed rates, reducing tool wear, and partly due to the increased contact stress on the surface of the tool subjected to larger cutting forces under higher feed rates, accelerating tool wear. Under these two combined effects, the tool life does not increase or decrease monotonically with feed rate. Hence, there also exists an optimal feed rate in terms of PCD tool life and machining quality in high-speed milling of Al6063/$SiC_p$/65p composites.

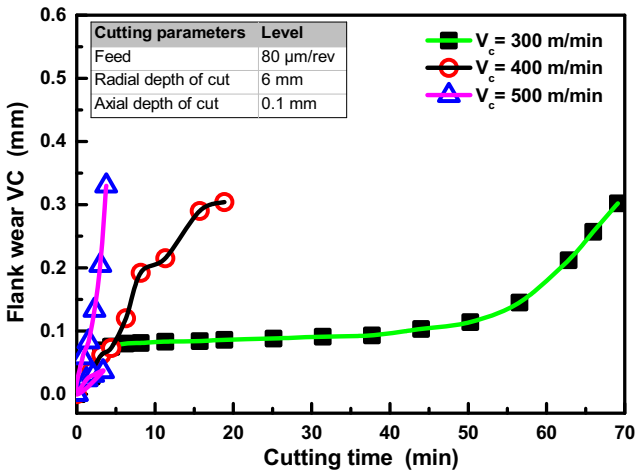


**Fig. 18** Influence of milling speed on flank wear

## 5 Conclusions

The aim of this work was to investigate the machinability of Al6063/$SiC_p$/65p composites reinforced with high-volume fraction of small-sized SiC particulates in high-speed end milling and provided systematic experimental study about cutting forces, thin-walled parts deformation, surface integrity, and tool wear during milling Al6063/$SiC_p$/65p composites. Based on the above analyses, the following main conclusions can be drawn:

1. The rotation, pressed-in, pulled-out, and fracture of SiC particulates lead to the formation of micro-crack, pits, swelling, and cavities. Moreover, the smearing of matrix material contributes to good surface quality. The machined surface morphologies reveal the cutting mechanism of SiC particulate plays an important role in defect formation mechanism on the machined surface.
2. When high-speed end milling Al6063/$SiC_p$/65p composites, the cutting forces are influenced considerably by feed rate and especially axial depth of cut, and the axial depth of cut plays a dominant role in the thin-walled parts deformation. The surface roughness of the Al6063/$SiC_p$/65p workpiece machined using 0.1-mm tool nose radius is slightly higher than that using 0.4-mm tool nose radius. The surface roughness increases with feed rate and axial depth of cut. Increased milling speed ranging from 100 to 240 m/min contributes to reducing the surface roughness, but will increase the surface roughness beyond this range. While performed high-speed cutting at 240 m/min, unlike concomitant movement of machined surface and sub-surface caused by the coordinated deformation during low-speed cutting at 100 m/min, as the unmachined surface was cut away, the machined surface and sub-surface suffered from less amount of deformation, thereby inducing less damage. The surface compressive residual stress

increases with increased feed rate and axial depth of cut. The surface compressive residual stress decreases from 113 to 94 MPa with the milling speed increasing from 100 to 240 m/min and increases from 94 to 113.5 MPa with the milling speed ranging from 240 to 380 m/min. This may be due to the synthetic action of tensile stress caused by heat generated during the milling process and compressive stress originating from mechanical deformation caused by cutting tool.

3. The tool morphologies of PCD too indicate microchipping, abrasive wear, graphitization, grain breaking off, and built-up edge are the dominated wear mechanism of PCD tool in high-speed milling dry milling of Al6063/$SiC_p$/65p composites. The change in milling speed affects the simultaneous changes in milling force and milling temperature, so its influence on tool wear and durability is the most pronounced. From the viewpoints of balancing machining cost and parts quality, it is feasible to select an optimal milling speed such as 300 m/min when high-speed milling of high volume fraction $SiC_p$/Al6063 composites in PCD tooling.
4. PCD tools with a larger nose radius contributes to a longer tool life, and a smaller diamond grain size can effectively extend tool life to some extent. There also exists an optimal feed rate in terms of PCD tool life and machining quality in high-speed milling of Al6063/$SiC_p$/65p composites. This may be partly due to the reduced probability of contact between SiC particulates and the tool flank under higher feed rates, reducing tool wear, and partly due to the increased contact stress on the surface of the tool subjected to larger cutting forces under higher feed rates, accelerating tool wear.

**Funding information** This work is supported by the National Natural Science Foundation of China under Grant No. 51575051.

## Compliance with ethical standards

**Conflict of interests** The authors declare that they have no conflict of interest.



## References

1. Dong Z, Zheng F, Zhu X, Kang R, Zhang B, Liu Z (2017) Characterization of material removal in ultrasonically assisted grinding of $SiC_p$/Al with high volume fraction. Int J Adv Manuf Tech 93(5–8):1–13
2. Hekner B, Myalski J, Pawlik T, Sopickalizer M (2017) Effect of carbon in fabrication Al-SiC nanocomposites for Tribological application. Materials 10(6)
3. Xiang J, Xie L, Gao F, Yi J, Pang S, Wang X (2018) Methodology for dependence-based integrated constitutive modelling: an illustrative application to SiCp/Al composites. Ceram Int 44(10):11765–11777
4. Han J, Hao X, Li L, Wu Q, He N (2017) Milling of high volume fraction $SiC_p$/Al composites using PCD tools with different structures of tool edges and grain sizes. Int J Adv Manuf Tech 92(5–8):1–8
5. Chen J, Gu L, Liu X, Zhao W (2018) Combined machining of SiC/Al composites based on blasting erosion arc machining and CNC milling. Int J Adv Manuf Tech 96(1–4):111–121
6. Chan KC, Cheung CF, Ramesh MV, Lee WB, To S (2001) A theoretical and experimental investigation of surface generation in diamond turning of an Al6061/$SiC_p$ metal matrix composite. Int J Mech Sci 43(9):2047–2068
7. Pramanik A, Zhang LC, Arsecularatne JA (2008) Machining of metal matrix composites: effect of ceramic particulates on residual stress, surface roughness and chip formation. Int J Mach Tool Manu 48(15):1613–1625
8. Ge YF, Xu JH, Yang H, Luo SB, Fu YC (2008) Workpiece surface quality when ultra-precision turning of $SiC_p$ /Al composites. J Mater Process Tech 203(1–3):166–175
9. Reddy NSK, Kwang-Sup S, Yang M (2008) Experimental study of surface integrity during end milling of Al/SiC particulate metal-matrix composites. J Mater Process Tech 201(1):574–579
10. Quan Y, Ye B (2003) The effect of machining on the surface properties of SiC/Al composites. J Mater Process Tech 138(1–3):464–467
11. El-Gallab M, Sklad M (1998) Machining of Al/SiC particulate metal matrix composites: part I: tool performance. J Mater Process Tech 83(1–3):151–158
12. El-Gallab M, Sklad M (1998) Machining of Al/SiC particulate metal matrix composites: part II: workpiece surface integrity. J Mater Process Tech 83(1–3):277–285
13. Li X, Seah WKH (2001) Tool wear acceleration in relation to workpiece reinforcement percentage in cutting of metal matrix composites. Wear 247(2):161–171
14. Dabade UA, Joshi SS, Balasubramaniam R, Bhanuprasad VV (2007) Surface finish and integrity of machined surfaces on Al/$SiC_p$ composites. J Mater Process Tech 192-193(1):166–174
15. Liu J, Wu J, Binner J (2017) Cutting resistance of metal-ceramic interpenetrating composites. Ceram Int 43(2):2815–2823
16. Huang S, Guo L, He H, Xu L (2018) Study on characteristics of SiCp/Al composites during high-speed milling with different particulate size of PCD tools. Int J Adv Manuf Tech 95(5–8):2269–2279
17. Zhou L, Wang Y, Ma ZY, Yu XL (2014) Finite element and experimental studies of the formation mechanism of edge defects during machining of $SiC_p$/Al composites. Int J Mach Tool Manu 84(6):9–16
18. Feng P, Liang G, Zhang J (2014) Ultrasonic vibration-assisted scratch characteristics of silicon carbide-reinforced aluminum matrix composites. Ceram Int 40(7:10817–10823
19. Zhou L, Cui C, Zhang PF, Ma ZY (2017) Finite element and experimental analysis of machinability during machining of high-volume fraction $SiC_p$/Al composites. Int J Adv Manuf Tech 91(5–8):1935–1944
20. Huang ST, Zhou L, Yu XL, Cui Y (2012) Experimental study of high-speed milling of $SiC_p$/Al composites with PCD tools. Int J Adv Manuf Tech 62(5–8):487–493
21. Bian R, He N, Li L, Zhan ZB, Wu Q, Shi ZY (2014) Precision milling of high volume fraction $SiC_p$/Al composites with monocrystalline diamond end mill. Int J Adv Manuf Tech 71(1–4):411–419
22. Xiang J, Xie L, Gao F, Zhang Y, Yi J, Wang T, Pang S, Wang X (2018) On multi-objective based constitutive modelling methodology and numerical validation in small-hole drilling of Al6063/$SiC_p$ composites. Materials 11(1):97

23. Xiang J, Pang S, Xie L, Gao F, Hu X, Yi J, Hu F (2018) Mechanism-based FE simulation of tool wear in diamond drilling of $SiC_p$/Al composites. Materials 11(2):252
24. Wang T, Xie L, Wang X, Ding Z (2015) PCD tool performance in high-speed milling of high volume fraction $SiC_p$/Al composites. Int J Adv Manuf Tech 78(9–12):1445–1453
25. Kannan S, Kishawy HA (2008) Tribological aspects of machining aluminium metal matrix composites. J Mater Process Tech 198(1): 399–406
26. Mondal DP, Ganesh NV, Muneshwar VS, Das S, Ramakrishnan N (2006) Effect of SiC concentration and strain rate on the compressive deformation behaviour of 2014Al-$SiC_p$ composite. Mat Sci Eng A-Struct 433(1–2):18–31
27. Xiang J, Xie L, Gao F, Yi J, Pang S, Wang X (2017) Diamond tools wear in drilling of $SiC_p$/Al matrix composites containing copper. Ceram Int 44(5):5341–5351